Extracted Power Optimization of Hybrid Wind-Wave Energy Converters Array Layout via Enhanced Snake Optimizer

Bo Yang [1], Miwei Li [1], Risheng Qin [2], Enbo Luo [2], Jinhang Duan [1], Bingqiang Liu [1], Yutong Wang [1], Jingbo Wang [3*], Lin Jiang [3]

[1] Faculty of Electric Power Engineering, Kunming University of Science and Technology, 650500 Kunming, China;

[2] Electric Power Research Institute, Yunnan Power Grid Company Ltd., 650217, Kunming, China;

[3] Department of Electrical Engineering and Electronics, University of Liverpool, L69 3GJ Liverpool, UK;

***** Correspondence: Jingbo Wang, E-mail: JingboWang96@outlook.com

Abstract: In recent years, wind energy and wave energy are widely concerned as highly developmental clean energy alternatives to traditional energy sources. From the perspective of cost reduction and power output enhancement, in this study, a V27-225kW wind turbine and wave energy converter are combined to construct a hybrid wind-wave energy converters (HWWEC), which greatly improves the power generation and operation stability. The optimization of wind-wave energy layout that involves strategically placing wave energy devices can directly influence the energy output of the whole system. To enhance the overall power generation efficiency, the optimal array configuration becomes a challenging but also promising solution regarding this concern. To optimize the array configuration that is composed of multiple HWWECS, this study develops an enhanced snake optimizer (ESO) based optimization scheme including chaotic initialization, asynchronous learning factors, and levy flight, which shows strong optimum searching ability while avoiding falling into local optimums. Simulation results under various case studies of three-line WECs consisting of three, six, and twelve buoys indicate that the ESO achieves the highest absorption power compared to other algorithms, particularly, the output power achieved by ESO is 144.337 kW higher than that obtained by the original SO.

Keywords: Enhanced snake optimizer, Hybrid wind-wave energy converter, Optimal layout configuration

Nomenclature			
Abbreviation		$B_{\mathrm{pto},\Sigma}$	damping block matrices of the PTO system
AEO	artificial ecosystem optimization	$\hat{x}_{\Sigma}$	acceleration vector of WEC
BAS	beetle antennae search	$\hat{F}_{\mathrm{exc},\Sigma}$	wave forces of excitation
ESO	enhanced snake optimizer	P_i	wave energy absorbed by single buoy
FWTS	floating wind turbine system	H	height of the wave
GWO	grey wolf optimizer	$\hat{I}_{i,j}$	motion amplitude of buoy
HWWEC	hybrid wind-wave energy converters	$P_{\mathrm{WEC},\Sigma}$	absorbed total power of *N* WECs
JS	jellyfish search	$X(\omega)$	displacement vector
PSO	particle swarm optimization	$C(\omega)$	damping coefficient
PTO	power take off	R	recovery coefficient
SO	snake optimizer	$F(\omega)$	additional force
WAMIT	wave analysis MIT software	$P_{\mathrm{WEC},\Sigma}$	absorbed total power of *N* WECs
WEC	wave energy converter	$A(\infty)$	additional mass at the wireless frequency
Variable		X	displacement

$V_{\text{cut\_in}}$	cut-in wind speed	X_1	velocity
V_{rated}	rated wind speed	X_2	acceleration respectively
$V_{\text{cut\_out}}$	cut-out wind speed	B_1	secondary viscous damping coefficient
$R(v)$	polynomial that fits the wind turbine power curve	$k(t-\tau)$	hysteresis
$P(v)$	power curve at a constant power W	$f(t, X, X_1)$	displacement and velocity function
P_{rated}	rated power	P_{Σ}	total absorbed power of a HWWECS array
M_{Σ}	mass matrix of the buoys	$P_{\text{FWT},\Sigma}$	absorbed power of FWT
ω	wave frequency	q	q factor
$A_{\Sigma}(\omega)$	radiating additional mass	P_0	absorbed power in isolation state
$B_{\Sigma}(\omega)$	damping coefficient matrix	N	number of HWWEC in an array
$K_{\text{pto},\Sigma}$	the stiffness of the PTO system		

1. Introduction

Nowadays, the acceleration and depletion of traditional energy consumption has prompted worldwide countries to seek and develop new energy candidates, which generally refers to renewable energy that are developed and utilized on the basis of new energy technologies, including wind energy, solar energy, wave energy, etc [1]. According to the latest global energy report, wind power accounts for 16% of global renewable energy generation, second only to hydropower. From the perspective of the global environment, the application of offshore wind power has increased significantly in the past decade. The installed capacity of offshore wind turbines has grown by approximately 21% annually since 2013 and is expected to reach 370GW by 2030, an increase of 85% compared to the forecast for 2021. In addition, the global share of new offshore wind capacity is expected to increase from 23% in 2021 to 30% in 2031 [3]. China's installed capacity of offshore wind power has witnessed a significant annual growth, reaching 3 GW and becoming the world's largest offshore wind power market for the third consecutive year [4]. Thanks to its environmentally friendly characteristics, wind power can reduce carbon dioxide, sulfur dioxide, and nitride emissions, thus promoting energy sustainability and protecting eco-environment [5]. Compared with onshore wind power generation, offshore wind towers are designed with lower height and higher ambient wind speed, whose main features are outlined as low wind shear, low turbulence, high production, wind turbine small loss, long service life, sea level, and no wind speed change. Offshore power generation also provides a foundation for the development of other marine resources. Meanwhile, offshore wind turbines are set up far away from the coast, as a result, the noise and visual interference are also very small [6]. Therefore, in the context of global pursuit of low-carbon economy, offshore wind power has shown great potential for its large-scale application. At the same time, wave energy, as one of the representative renewable energy sources, has also been highly concerned and valued over the last decade [7],[8]. Wave power generation technology is developed based on the existing research and application scenarios, using the effective combination of mature mechanical manufacturing and power generation technology. Coastal wave energy storage is extremely huge, while its production and utilization has only little impact on the environment. Wave energy based power generation shows high time utilization rate and low power generation cost, which also shows high predictability thanks to its small long-distance transmission energy dissipation, long transmission distance, and high energy density [9]. The development of wave

energy not only aims to improve energy shortage condition, but also to more reasonably utilize marine energy [10].

Chandrasekaran and Sricharan note that the annual energy production correlates with a trend toward the Levelized Cost of Electricity, which shows a promising future for hybrid systems as the cost of electricity increases [11]. To this end, considering the appropriate use of wave field space, the installation of offshore wind power on the WEC system can make more efficient utilization of offshore space via hybrid wind and wave energy converter (HWWEC), which owns prominent practical value and promising future [12]. Moreover, floating wind turbine systems (FWTS) and wave energy converters (WEC) devices can share infrastructure such as brackets, cables, and transmission systems on the same platform, thus overall establishment cost of the system can be reduced. Meanwhile, monitoring, maintenance, and management resources can be shared between the two systems, such that the operation and maintenance (O&M) costs can also be decreased. In addition, FWTS power generation is affected by local wind speed, and WEC power generation is affected by wind and wave conditions. The combination of the two can provide a more stable energy output in different weather conditions. Furthermore, considering that current wave farms mainly supply power to coastal areas or isolated islands, combining wave energy with other renewable resources, such as FWTS, is a reliable way to generate electricity and power for remote areas. However, such hybrid systems need to be coupled to complex marine environments, which challenges the reliability of HWWEC systems. Thus far, a variety of related research has been presented, for instance, literature [13] combines the heave type point absorber wave energy converter (WEC) with TLP-based oscillating water column, which can reduce the amplitude of TLP motion. Literature [14] establishes a new mixed wave system and analyzes its hydrodynamic characteristics in regular and irregular waves. Literature [15] devises a tumbler-shaped hybrid triboelectric nanogenerator, which can simultaneously capture wind and wave energy in the ocean. In reference [16], a new type of hydraulically driven wind and wave hybrid power generation device is developed to improve the stability of the system's output power.

In general, HWWEC can be deployed as a cluster to collect power for commercial and large-scale power generation, during which the wave energy distribution optimization plays a crucial role in maximizing energy production, reducing cost, and decreasing environmental impact of HWWECS. The optimization of wave energy layout involves strategically placing the wave energy device in a position with large wave potential, which requires comprehensive consideration of various factors such as equipment characteristics, wave properties, water depth, seabed conditions, and proximity to power infrastructure [17]-[21]. To maximize the absorbed power, the optimization of array configuration becomes the core step to improve the energy output and conversion efficiency of HWWECs [22][23]. Budal started the study of array layout optimization in 1977, which is still a popular and widespread research topic thus far, in which the arrangement of device parameters in the wave field is crucial [24],[25]. Silvia Bozzi [26] investigates the hydrodynamic interaction among WECs in different distances and different layouts, which also proves that these negative impacts can therefore be mitigated through the strategic placement of wave energy devices to ensure the sustainability of the marine environment. Today, research on modelling and performance analysis of this hybrid system is still ongoing. Peng Jin et al. propose a novel DeepCWind-Wave Stars hybrid system the layout of the Wave Stars is optimized, Under each wind condition (wind speed U = 0, 8 m/s, 11.4 m/s, and 14 m/s), the Wave Stars can provide power over 500 kW, which is highly valuable for the entire system during wind turbine downtime [27]. In reference [12], a

comprehensive numerical hybrid model is developed that can tackle the full couplings by bridging the aerodynamic module of OpenFAST and the hydrodynamic simulator WAFDUT through an in-house code based on multi-body dynamics. The array of this model can generate over 500 kW wave power in the waves with periods of 6 s-10 s, which can be a qualified supplement to wind power. Literature [28] proposes a hybrid Wavestar-DeepCwind platform, which is composed of Wavestar WEC and a floating wind turbine to evaluate the power matrix under different regular wave conditions and different Wavestar diameters. Numerical results indicate that the maximum absorbed power and maximum capture width ratio can be obtained around the wave periods (T = 5s and T = 6s) for all wave heights (H = 1-4m) and Wavestar diameters (D = 5-10m).

Currently, the methods regarding the optimal configuration of wave energy converter (WEC) array layout can be divided into three main categories: meta-heuristic, machine learning, and mathematical method [29]. Among them, with the rapid development of computer science, various researches on HWWEC optimization configuration based on meta-heuristic methods have made solid progress and achieved remarkable achievements, including particle swarm optimization (PSO), greedy algorithm, multi-objective lightning search algorithm, and many hybrid variants [25]. Compared with traditional analytical methods, meta-heuristic algorithm shows much more notable optimization accuracy and speed when solving complex and highly nonlinear problems [30][32]. A preliminary study of the effect of array layout on the total output power of WEC has been carried out by Child and Venugopal in 2010, in which the standard genetic algorithm (GA) and parabolic crossover methods are combined to optimize the WEC layout. Afterward, literature [33] applies GA to optimize the array layout based on the hydrodynamic model while containing the array cost. Besides, reference [34] adopts the differential evolution algorithm for multi-parameter optimization of a WEC square array, which shows distinctive optimization stability.

Though some positive progress has been achieved in the aforementioned studies, at present, the layout optimization of HWWEC models still lacks an in-depth study in terms of both model analysis and optimization algorithm design. Therefore, in response to this problem, this work develops an enhanced snake optimizer (ESO) to realize optimal layout configuration of HWWEC, whose contributions are summarized as follows:

(1) A new HWWEC based on a V27-225kW wind turbine [35] is proposed, which has three series of WEC and power take-off (PTO) in the frequency domain based on fluid dynamics model under constant power. The proposed HWWEC is adopted as a hybrid wind and wave system model, in which the q-factor is introduced as an optimization evaluation index [36];
(2) The original SO [37] is improved as ESO by introducing chaotic initialization, asynchronous learning factors, and Levy flight [38], which increases the global convergence performance and the system's output power;
(3) Three-line WECs consisting of three, six, and twelve buoys are employed for performance validation and analysis, upon which six other advanced algorithms apart from ESO are also employed as the comparative algorithms including the original SO, ecosystem optimization (AEO), jellyfish search (JS), grey wolf optimizer (GWO), beetle antennae search (BAS), and particle swarm optimization (PSO) for a comprehensive evaluation.

The remaining of this study is structured as follows: Section 2 describes the mathematical model of HWWEC. Section 3 introduces the mechanism of SO and ESO. Section 4 discusses the implementation of HWWEC layout optimization based on ESO. Section 5 undertakes case studies and analysis. Section 5 concludes the whole work.

2 Hybrid Wind-Wave Energy Converter Modeling

In this section, the HWWEC consists of floating wind turbine system and WEC system as well as the optimization evaluation index of HWWEC system, are discussed.

2.1 Dynamics analysis

Dynamics analysis includes the power generation of Vestas V27-225 kW floating wind turbine system at average wind speed and the three-series WEC array model.

2.1.1 Floating wind turbine system

The floating wind turbine uses Vestas V27-225 kW (rotor diameter: 27 m) to estimate the theoretical annual power generation, whose main parameters are outlined in Table 1. According to the data monitoring proposed in the study developed by Jaramillo et al. [39], the average wind speed is 10.56 m/s. The wind power output of the wind power system is determined by the corresponding power curve. Between the rated speed and the cut-off speed, the power curve $P(v)$ of the Vestas V27-225 kW wind turbine running at a constant power P_{rated} can be expressed as

$$P(v)=\begin{Bmatrix} 0, & v<V_{\text{cut\_in}} \\ P_{\text{rated}}*R(v), & V_{\text{cut\_in}}\le v<V_{\text{rated}} \\ P_{\text{rated}}, & V_{\text{rated}}\le v<V_{\text{cut\_out}} \\ 0, & V_{\text{cut\_out}}<v \end{Bmatrix} \tag{1}$$

where v is the wind speed, $V_{\text{cut\_in}}$, V_{rated} and $V_{\text{cut\_out}}$ are the cut-in, rated, and cut-out speeds, respectively; P_{rated} is the rated power of the wind turbine; $R(v)$ is a polynomial function that ideally fits the wind turbine power curve for regression, the relationship between the polynomial function $R(v)$ and the rated power P_{rated} of the wind turbine is normalized in this case.

For Vestas V27-225 kW fans (rated P_{rated}=225 kW), the ideally fitted power curve $R(v)$ can be expressed by

$$R(v)=\left[a_2+\frac{a_1-a_2}{1+\exp(\frac{v-a_3}{a_4})}\right] \tag{2}$$

where v is the ambient wind speed.

Table 1. Main parameters of floating wind power system

The regression constant, the cut in, rated and cut-out speed of the turbine power curve	
$a_1=-0.031$	$V_{\text{cut\_in}}=3.5[\text{m/s}]$
$a_2=1.073$	$V_{\text{rated}}=11.0[\text{m/s}]$
$a_3=9.006[\text{m/s}]$	$V_{\text{cut\_out}}=22.5[\text{m/s}]$
$a_4=1.779[\text{m/s}]$	$\text{P}_{\text{rated}}=225[\text{kW}]$

2.1.2 Wave energy converter system

Wave energy converter system plays a key role in converting wave energy into electrical energy, which consists of WEC, PTO systems, and other auxiliary systems. It is noteworthy that the three-series WEC array model adopted in this work can be denoted by a dynamic equation derived in the frequency domain based on the conditions of invisticity, irrotation, and incompressibility of seawater. The small amplitude motion caused by the geometrical arrangement of the three-tethered

WEC is ignored, and only the translational motion of each system is considered.

The dynamic equation of WEC in the frequency domain can be described by [36]

$$\left((M_{\sum}+A_{\sum}(\omega))j\omega+B_{\sum}(\omega)-\frac{K_{\mathrm{pto},\sum}}{\omega}j+B_{\mathrm{pto},\sum}\right)\hat{x}_{\sum}=\hat{F}_{\mathrm{exc},\sum} \tag{3}$$

where the subindices represent the generalized vectors/matrices of *N* WEC arrays; $M_{\sum}$ is the mass matrix of the buoys; ω is the frequency of the wave; $A_{\sum}(\omega)$ and $B_{\sum}(\omega)$ are the radiating additional mass and damping coefficient matrix, respectively, containing the fluid east-west interaction between the buoys; $K_{\mathrm{pto},\sum}$ and $B_{\mathrm{pto},\sum}$ are the stiffness and damping block matrices of the PTO system, respectively; $\hat{x}_{\sum}$ is the acceleration vector of WECs.

The wave energy P_i absorbed by single buoy of WECs in the frequency domain is:

$$P_i=\sum_{j=1}^{3}\frac{1}{2}B_{\mathrm{pto},i}\omega^2H^2\left|\hat{l}_{i,j}\right|^2 \tag{4}$$

where $B_{\mathrm{pto},i}$ is the damping coefficient matrix of the PTO device; *H* is the height of the wave; $\left|\hat{l}_{i,j}\right|$ is the motion amplitude of the buoy on the square side of the tether.

The total power of wave energy absorbed by the buoys containing *N* WECs is expressed as follows：

$$P_{\mathrm{WEC},\sum}=\frac{1}{4}(\hat{F}^{*}_{\mathrm{exc},\sum}\hat{\dot{x}}^{*}_{\sum}\hat{F}_{\mathrm{exc},\sum})-\frac{1}{2}\hat{\dot{x}}^{*}_{\sum}B_{\mathrm{pto},\sum}\hat{\dot{x}}_{\sum} \tag{5}$$

where symbol $*$ express as the transpose of the matrix variable.

2.1.3 Hybrid wind-wave energy converter system

As shown in Fig. 1, HWWEC is composed of floating wind turbine system (FWTS) and WEC which is based on the simulation model of aerodynamic-servo-hydroelasticity in frequency domain. Among them, the Rotor diameter of the FWTS is 27m, the Hub height is 32.1m, and the WEC device is 6m from the sea level [40]. The hydrodynamic characteristics of a rigid body, including six degrees of freedom and potential damping, are constructed by using wave analysis MIT (WAMIT) software, which effectively shows the effect of WEC on the hybrid wind-wave energy converter system under the condition of regular wave motion. The equation of motion based on linear potential flow theory considering nonlinear effects is described as follows [41]-[43]:

$$-\omega^2\{M+A(\omega)\}X(\omega)+i\omega C(\omega)X(\omega)+RX(\omega)=F(\omega) \tag{6}$$

where *M* is the structural mass; $X(\omega)$ is the displacement vector; $C(\omega)$ is the damping coefficient; *R* is the recovery coefficient; $F(\omega)$ is the additional force.

Consider the motion equation of the cylinder block with secondary viscous damping based on six degrees of freedom in the time domain as follows:

$$\{M_{\mathrm{HWWEC}}+A(\infty)\}X_2(t)+B_1X_1|X_1|+\int_0^t k(t-\tau)X(\tau)\mathrm{d}\tau+RX(t)=f(t,X,X_1) \tag{7}$$

where $A(\infty)$ is the value of the additional mass at the wireless frequency; X, X_1, X_2 denote the displacement, velocity, and acceleration respectively; B_1 is the secondary viscous damping coefficient, $k(t-\tau)$ is the hysteresis function; $f(t,X,X_1)$ is the displacement and velocity function.

Assuming that there are *N* HWWECs devices in the array, and the wave frequency, wave height, wind speed, wind direction, etc., the total power absorbed by an HWWECs array is presented by

$$P_{\sum}=P_{\mathrm{WEC},\sum}+P_{\mathrm{FWT},\sum} \tag{8}$$

where $P_{\sum}$ is total absorbed power of a HWWECs array; $P_{\mathrm{FWT},\sum}$ is absorbed power of FWTs.

2.2 Performance index

The optimization comparison among different HWWECs arrays uses q factor as the specific parameter evaluation index, and its expression is expressed as follows [36]:

$$q = \frac{P_{\Sigma}}{N \cdot P_0} \tag{9}$$

where P_0 is the absorbed power in isolation state; P_{Σ} is the power absorption value of a group of HWWECs; when the q factor is greater than 1, it indicates that there is constructive interference in the array, which is beneficial to the overall energy generation of the system; on the contrary, when the q factor is less than 1, there is destructive interference, which is harmful to the overall system.

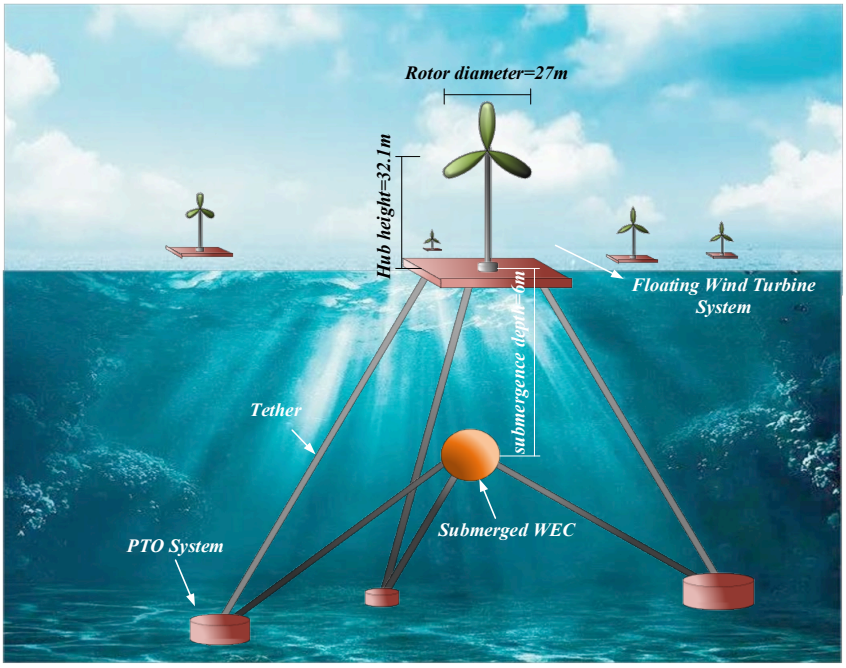

Fig.1. Hybrid wind-wave energy converter system

3. Enhanced Snake Optimizer

SO shows acceptable effectiveness and efficiency in terms of balance between exploration and exploitation, however, the algorithm itself is also limited by its inherent limitations, e.g., easily falling into local optimal solutions. Therefore, this section designs an improved SO called ESO to improve its overall optimization ability by introducing three mechanisms.

3.1 Snake optimizer

SO mainly replicates the mating behaviors of snakes, i.e., snakes tend to mate when the temperature is low and food is abundant, otherwise, they will only search for food. Thus, based on this behavior patterns of snakes, the searching process of SO is divided into two stages: exploration and exploitation.

Firstly, the initialized population is divided into two sub-populations, female and male groups, accounting for about 50% of the total number, respectively, that is [37]:

$$N_{\mathrm{f}} = N/2 \tag{10}$$

$$N_{\mathrm{m}} = N/2 \tag{11}$$

where N is population size; N_{f} is the number of female individuals; N_{m} is the number of male individuals.

In the divided male and female sub-populations, the optimal individual in the corresponding sub-populations is pinned, respectively. The best male individual $f_{\mathrm{best,m}}$, the best female individual $f_{\mathrm{best,f}}$, and their corresponding food position f_{food} are then obtained. In addition, the food quantity Q and temperature *Temp* are defined, which can be expressed as:

$$Temp = \exp(\frac{-t}{T}) \tag{12}$$

$$Q = c_1 * \exp(\frac{t-T}{T}) \tag{13}$$

where t represents the current number of iterations; T represents the maximum number of iterations, which can ensure that the temperature is gradually reduced on the whole; c_1 is a constant, and its value is equal to 0.5.

The aforementioned formulas can ensure that the amount of snake food increases with iterations, which can provide a positive environment for subsequent snake mating behavior. In the exploration phase, under the influence of low ambient temperature (food quantity Q<0.25), the snake only searches for food in the current environment (local search). Snakes search for food through any location and update their location based on the following equations:

$$x_{i,\mathrm{m}}(t+1) = x_{rand,\mathrm{m}}(t) \pm c_2 * A_{\mathrm{m}} * ((x_{\max} - x_{\min}) * rand + x_{\min}) \tag{14}$$

$$x_{i,\mathrm{f}}(t+1) = x_{rand,\mathrm{f}}(t) \pm c_2 * A_{\mathrm{f}} * ((x_{\max} - x_{\min}) * rand + x_{\min}) \tag{15}$$

$$A_{\mathrm{m}} = \exp(\frac{-f_{rand,\mathrm{m}}}{f_{i,\mathrm{m}}}) \tag{16}$$

$$A_{\mathrm{f}} = \exp(\frac{-f_{rand,\mathrm{f}}}{f_{i,\mathrm{f}}}) \tag{17}$$

where c_2 is a constant and its value is equal to 0.05; A_{m} and A_{f} are the ability of male snake and female snake to find food; $f_{rand,\mathrm{m}}$ and $f_{rand,\mathrm{f}}$ are the fitness values of $x_{rand,\mathrm{m}}$ and $x_{rand,\mathrm{f}}$, respectively; $f_{i,\mathrm{m}}$ and $f_{i,\mathrm{f}}$ are the fitness values of $x_{i,\mathrm{m}}$ and $x_{i,\mathrm{f}}$, respectively; rand denotes a random value between 0 and 1.

In the exploitation stage, when food is abundant (food quantity Q>0.25), the decision to continue searching for more food or to find females to mate is made according to the ambient temperature (global search).

When the temperature *Temp*>0.6, then the temperature is high, the snake will only continue foraging, and the position formula is updated as follows:

$$x_{i,j}(t+1) = x_{\mathrm{best}} \pm c_3 * Temp * rand * (x_{\mathrm{food}} - x_{i,j}(t)) \tag{18}$$

where $x_{i,j}$ is the position of the snake (female or male); x_{best} is the best position for snakes; c_3 is a constant whose value is equal to 2.

When the temperature *Temp*<0.6, then the temperature is low, snakes will mate or fight.

a) Mating model

The positions of male and female snakes when mating are updated as follows:

$$x_{i,\mathrm{m}}(t+1) = x_{i,\mathrm{m}}(t) + c_3 * M_{\mathrm{m}} * rand * (Q * x_{i,\mathrm{f}}(t) - x_{i,\mathrm{m}}(t)) \tag{19}$$

$$x_{i,\mathrm{f}}(t+1) = x_{i,\mathrm{f}}(t) + c_3 * M_{\mathrm{f}} * rand * (Q * x_{i,\mathrm{m}}(t) - x_{i,\mathrm{f}}(t)) \tag{20}$$

$$M_{\mathrm{m}} = \exp(\frac{-f_{i,\mathrm{f}}}{f_{i,\mathrm{m}}}) \tag{21}$$

$$M_{\mathrm{f}} = \exp(\frac{-f_{i,\mathrm{m}}}{f_{i,\mathrm{f}}}) \tag{22}$$

where $x_{i,\mathrm{m}}$ and $x_{i,\mathrm{f}}$ are the positions of the *i*th male and female respectively; M_{m} and M_{f} represent the mating ability of males and females, respectively; $f_{i,\mathrm{m}}$ and $f_{i,\mathrm{f}}$ are divided into the *i* individual fitness of male and female.

If the eggs hatch, the worst male and female individuals in the population are selected for replacement as follows:

$$x_{\mathrm{worst,m}} = x_{\min} + rand * (x_{\max} - x_{\min}) \tag{23}$$

$$x_{\mathrm{worst,f}} = x_{\min} + rand * (x_{\max} - x_{\min}) \tag{24}$$

where $x_{\mathrm{worst,m}}$ are the worst individuals in the male group; $x_{\mathrm{worst,f}}$ are the worst individuals in the female group.

b) Fight mode

The position of the battle mode is updated as follows:

$$x_{i,\mathrm{m}}(t+1) = x_{i,\mathrm{m}}(t) + c_3 * FM * rand * (Q * x_{\mathrm{best,f}} - x_{i,\mathrm{m}}(t)) \tag{25}$$

$$x_{i,\mathrm{f}}(t+1) = x_{i,\mathrm{f}}(t) + c_3 * FF * rand * (Q * x_{\mathrm{best,m}} - x_{i,\mathrm{f}}(t)) \tag{26}$$

$$FM = \exp(\frac{-f_{\mathrm{best,f}}}{f_i}) \tag{27}$$

$$FF = \exp(\frac{-f_{\mathrm{best,m}}}{f_i}) \tag{28}$$

where $x_{i,\mathrm{m}}$ and $x_{i,\mathrm{f}}$ are the positions of the *i*th male and female; $\mathrm{x}_{\mathrm{best,f}}$ and $\mathrm{x}_{\mathrm{best,m}}$ are the best positions of the *i*th female and male, respectively; *FM* and *FF* are the fighting abilities of male and magnetic snakes, respectively; $f_{\mathrm{best,f}}$ and $f_{\mathrm{best,m}}$ are the best individual fitness of magnetic snakes and male clubs, respectively; f_i is the fitness value of individual *i*.

3.2 Enhanced Snake Optimizer

During exploration and exploitation phases, the parameters of SO are fixed due to the limits of natural law. Considering that this limitation causes SO to easily fall into local optimums and reduce convergence speed, this study introduces chaotic initial population to improve the initial population diversity. Meanwhile, asynchronous learning factors are applied instead of fixed parameters, which is beneficial for jumping out of the limitation of natural laws and providing higher searching diversity and global convergence rate with levy flight.

3.2.1 Chaotic initial population

The main idea of chaos search is to produce chaotic sequence in some iterative way. Generally, the logistic equation is used to produce chaotic sequence [38]:

$$y(k+1) = \mu y(k)(1 - y(k)), \mu \in [0,4], y \in [0,1] \tag{29}$$

where μ is the bifurcation parameter of the logical map, the chaotic effect is the best when μ takes 4.

3.2.2 Asynchronous learning factors

The variable step learning factor is adopted to dynamically adjust the fixed constant in the algorithm according to the number of iterations. This mechanism can expand the searching range and avoid the local optimal solution. The constant c is improved as follows:

$$c_1 = c_{1,\text{start1}} + (c_{1,\text{end1}} - c_{1,\text{start1}}) * \frac{t}{T_{\max}} \tag{30}$$

$$c_2 = c_{2,\text{start2}} + (c_{2,\text{end2}} - c_{2,\text{start2}}) * \frac{t}{T_{\max}} \tag{31}$$

$$c_3 = c_{3,\text{start3}} + (c_{3,\text{end3}} - c_{3,\text{start3}}) * \frac{t}{T_{\max}} \tag{32}$$

where c_{start} and c_{end} are two constants; t is number of current iterations; $T_{\max}$ is the maximum number of iterations.

3.2.3 Levy flight

Levy flight strategy is introduced to update the individual position by simulating the flight behavior of whales in the search process, which is mainly used to jump out of the local optimal solutions, expand the searching range, and improve the global searching ability of the algorithm. The improvement formula is designed as follows:

$$x_i(t+1) = x_{i,\text{best}}(t) + \text{Levy}(d) * (x_{\text{best}}(t) - x_i(t)) \tag{33}$$

$$\text{Levy}(d) = 0.01 * \frac{r_1 * \sigma}{|r_2|^{1/\beta}} \tag{34}$$

$$\sigma = \left\{ \frac{\text{gama}(1+\beta) * \sin(\pi\beta/2)}{\text{gama}[(1+\beta)/2] * \beta * 2^{(\beta-1)/2}} \right\}^{1/\beta} \tag{35}$$

where d is the vector dimension; $x_{i,\text{best}}$ is the optimal solution of the first time; r_1 and r_2 are random values from 0 to 1 respectively; gama is a gamma function; β is taken at 1.5.

3.2.4 Enhanced snake optimizer

The improvement in ESO is based on three mechanisms, namely, chaos optimization algorithm, asynchronous learning factors, and Levy flight. Firstly, chaos optimization algorithm is used to improve the population initialization, expand the searching range of initialization, and find the initial optimal solution of male and female snakes.

Secondly, the asynchronous learning factor mechanism is used to optimize the constants c_1, c_2 and c_3 in algorithm's position update formula, as follows:

$$c_1 = c_{\text{start1}} + (c_{\text{end1}} - c_{\text{start1}}) * \frac{t}{T} \tag{36}$$

$$c_2 = c_{\text{start2}} + (c_{\text{end2}} - c_{\text{start2}}) * \frac{t}{T} \tag{37}$$

$$c_3 = c_{\text{start3}} + (c_{\text{end3}} - c_{\text{start3}}) * \frac{t}{T} \tag{38}$$

where c_{start1}, c_{start2} and c_{start3} are taken at 0.5, 0.05, and 2 respectively; c_{end1}, c_{end2}, and c_{end3} are taken at 0.5.

Finally, to avoid the shortcoming of original SO algorithm, i.e., easily falling into local optimal solutions and resulted low convergence accuracy, Levy flight mechanism is introduced in ESO to more thoroughly explore the global space of solutions to avoid local optimums.

4. Optimal Array Layout Design of WECs based on Enhanced Snake Optimizer

The application of the proposed ESO to the layout optimization of HWWECs is to continuously update the array until finding the optimal location of each device corresponding to the best fitness. In this work, ESO is proposed to optimize the arrangement of HWWECs to maximize the total power output, and to add constraints for a more accurate application of ESO.

4.1 Fitness function

To evaluate the optimization performance of each algorithm more quantitatively for HWWECs, thus further determining the optimal array position arrangement and the maximum power generated by the array to improve the wave energy capture ability of WEC arrays, this work uses the q factor to present the optimization performance of each algorithm, that is, to find the maximum q factor value. Thus, the fitness function is defined as:

$$\begin{cases} q_{\text{best}} = \max(q_1, q_2, \ldots, q_n), 1 \le n_{\max} \\ q = \dfrac{P_\Sigma}{N * P_0} \end{cases} \tag{39}$$

4.2 Constraint condition

In practical engineering, a safe distance between array buoys is required to facilitate installation and maintenance, so the safe distance between the buoys should be set longer than or equal to 50 meters and installed within the specified sea area under the constraints:

$$\begin{cases} x_i \in (0, width_{\max}), i = 1,2,\ldots,n \\ y_i \in (0, height_{\max}), i = 1,2,\ldots,n \\ d_{\text{safe}} = \sqrt{(x_i - x_j)^2 + (y_i - y_j)^2} \ge 50, i, j = 1,2,\ldots,n, i \ne j \end{cases} \tag{40}$$

where x_i and y_i are the coordinate values of the buoy respectively; $width_{\max}$ and $height_{\max}$ are the maximum length and height of the sea area respectively; and d_{safe} is the constraint distance between the buoys.

4.3 Optimization process of WEC array arrangement based on the enhanced snake algorithm

From Table 2 and Fig. 2, it can be observed that for ESO based optimization of WECs array, the key optimization parameters are all specifically defined. The optimization involves chaos random initialization, the optimal fitness value, and position selection, SO and Levy flight mechanism based position updating, and the final best fitness value determination along with its corresponding position. In addition, if the boundary value is exceeded during the update position process, a random value will be reassigned within the range.

Table 2. Pseudocode of ESO based WECs array optimization

1: **INPUT :** N(number of male and female population),Ub(upper bound variable),Lb(lower bound variable),T_{max}(maximum number of iterations),dim(dimensional variable).
2: Chaotic initial population by Eq.(29) ;Divide population N to 2 equal groups N_m and N_f using Eq.(10)and Eq.(11).
3: Calculate the fitness of each individual by Eqs.(4)-(8); Save the best fitness q_{best} and corresponding position x_{best}.
4:**WHILE** $t \leq T_{max}$
5: Evaluate each group N_m and N_f.
6: Find best male $f_{best,m}$ and best female $f_{best,f}$.
7: Define *Temp* using Eq.(12).
8: Define food quantity Q using Eq.(13).
9: **IF** (Q<0.25)
10: Perform exploration using Eqs.(14)-(17).
11: **EISE IF** (*Temp*>0.6)
12: Perform development using Eq.(18).
13: **EISE**
14: **IF** (*rand*<0.6)
15: Snake location update in mating pattern by Eqs.(19)-(24).
16: **EISE**
17: Snake location update in fight pattern by Eqs.(25)-(28).
18: **END IF**
19: **END IF**
20: Update location with the levy flight; Calculate the best male and female fitness by Eqs.(33)-(35).
21:**END WHILE**
21:**OUTPUT:**Best position and the best solution.

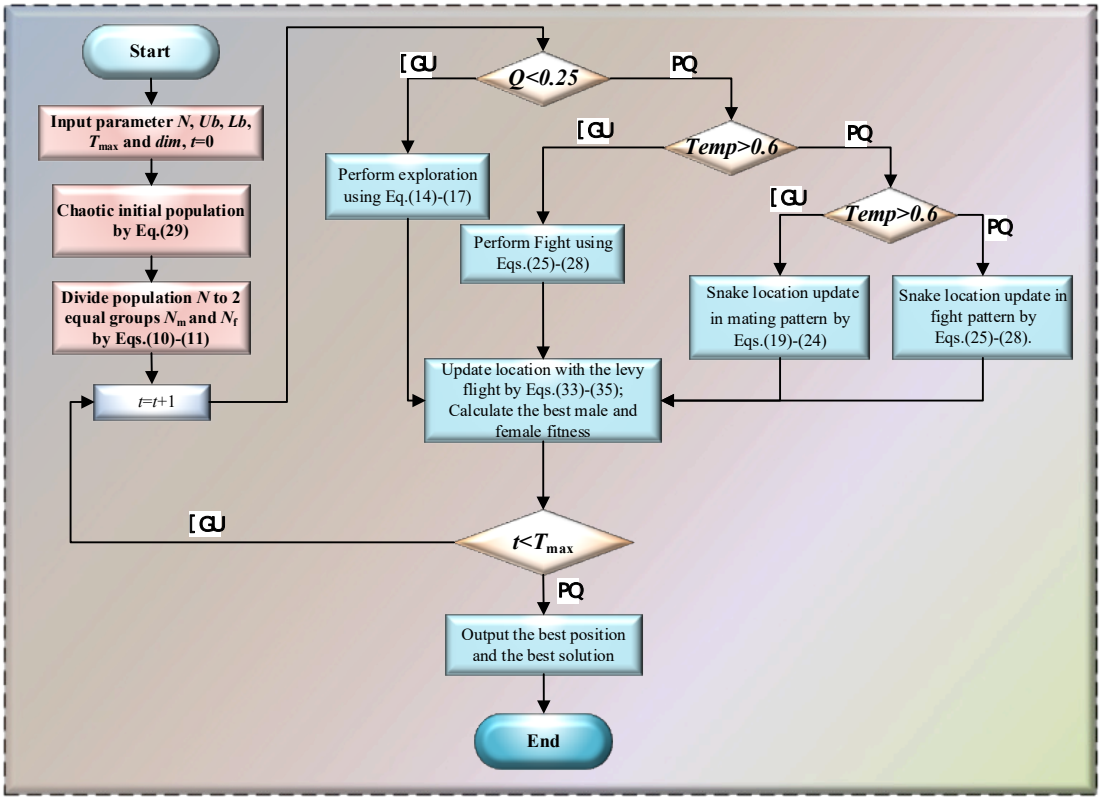

Fig.2. Flowchart of ESO algorithm

5. Case Studies

In this study, for a comprehensive evaluation, six other advanced algorithms apart from ESO are also selected as the comparative algorithms including the original SO, AEO, JS, GWO, BAS,

and PSO, to verify the array optimization capability for three-line WECs consisting of three, six, and twelve buoys, respectively. The surroundings of WECs in the three systems are set as the average wind speed is 10.56 m/s, the wave height is 1.9 m, the wave frequency is 0.7 rad/s, the incidence angle is 0 rad, and the wind speed spreads from left to right. To save the calculation costs, the wave conditions at 1 frequency are used [41], and the sea areas at the three scales are 400*400 m^2, 800*800 m^2, and 1600*1600 m^2, respectively. All algorithms run independently 20 times, meanwhile, considering the computational cost, population size and maximum iterations are respectively set as n=50 and T=400. All simulations are executed under the same conditions, i.e., the processor is AMD Ryzen 7 5700G with Radeon Graphics 3.80 GHz under 64-bit OS Windows 10 with memory 64.0 GB, and the software is MATLAB R2021b. The main parameters of each algorithm are tabulated in Table 3, and Table 4 shows the main parameter settings of the WECs system:

Table 3. The main parameters of seven algorithms

Algorithms	Parameter	Value
ESO	c_{start1}	0.5
	c_{start2}	0.05
	c_{start3}	2
	c_{end1}	0.5
	c_{end2}	0.5
	c_{end3}	0.5
	β	1.5
SO	c_1	0.5
	c_2	0.05
	c_3	2
	β	1.5
PSO	c_1	1.49445
	c_2	1.49445
JS	B	3
	γ	0.1
BAS	ε	0.95

Table 4. The main parameter settings of the WECs system

Parameter categories	Value
Buoy radius (m)	5
Buoy weight (kg)	3.76×10^5
Submergence depth H_{sub} (m)	6
PTO spring coefficient K_{pto} (kN/m)	387
PTO damping coefficient B_{pto} (kN/m)	161
Water density ρ_β (kg/m^3)	1020
Gravitational acceleration g (m/s^2)	9.81
Wave height H_{wave} (m)	1.9
Wave-wind propagation angle θ (rad)	0

5.1 Scenario 1: three buoys array

Scenario 1 is based on the location optimization of seven algorithms with a sea area of 400*400 m^2. Figure 3 shows the results of the change of q factor with iterations and box plot of each algorithm under small-scale of the three buoys.

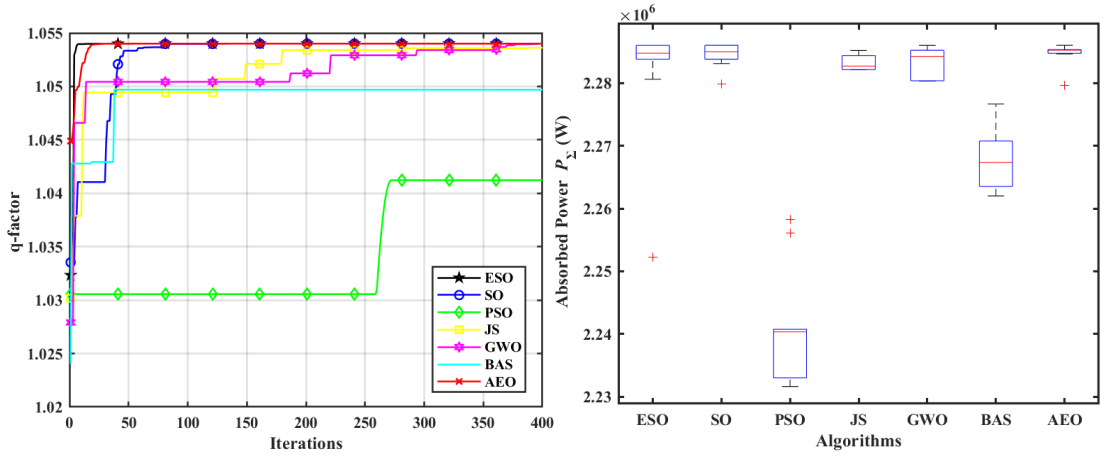

(a) (b)

Fig.3. Simulation results of seven algorithms under three buoys array. (a) q factor and (b) box plot.

Table 5. Simulation results of seven algorithms under three buoys array

Algorithms	Buoy number i	X/m	Y/m	P_i/kW	P_Σ/MW	q factor	T_{avg}/s
ESO	1	390.72	205.14	730.066	2.2861	1.054	4240
	2	206.10	390.63	787.489			
	3	329.71	80.118	768.474			
SO	1	161.52	327.08	768.456	2.2860	1.054	4240
	2	37.77	16.52	787.512			
	3	222.54	202.13	730.062			
PSO	1	143.03	126.13	754.025	2.2583	1.0412	4440
	2	152.18	234.25	739.923			
	3	142.47	318.70	764.369			
JS	1	348.44	200.05	730.184	2.2852	1.0536	4240
	2	284.70	75.14	768.322			
	3	160.50	383.05	786.650			
GWO	1	315.61	350.02	768.427	2.2860	1.054	4740
	2	192.11	39.19	787.509			
	3	377.21	225.18	730.083			
BAS	1	330.17	5.28	763.070	2.2767	1.0497	11050
	2	383.37	134.75	727.158			
	3	216.69	310.82	786.446			
AEO	1	224.41	339.98	768.456	2.2860	1.054	8325
	2	285.44	215.03	730.063			
	3	100.66	29.42	787.511			

According to the definition and changing principle of q factor, when q factor of the seven algorithms is greater than 1, indicating that the array-optimized WECs system has higher wave absorption energy at the same number of buoys. It is not difficult to see that from Fig. 3(a), except

for PSO JS and BAS, the other six algorithms can find the optimal solution q=1.0540 at different speeds, and ESO, SO, GWO, and AEO find the optimal solution at the 7th, 80th, 38th, and 24th times, respectively, which fully proves that ESO has the fastest speed and the highest optimization accuracy among ESO, SO, BAS, and AEO. According to Fig. 3(b), the power fluctuations of ESO, SO, JS, GWO, and AEO after 20 times are small, with a high median and fewer outliers, indicating that the optimization results of these five algorithms are stable.

Table 5 summarizes the optimization results of seven algorithms under the case of three buoys, including the best position, the optimal total absorbed power, the absorbed power of each buoy, and q factor. ESO shows the highest absorbed power while PSO obtains the lowest absorbed power, with a difference of 27.8kW between them. Fig. 4 shows the optimal layout of the seven algorithms under the optimal absorbed power. At the same time, under this scale, the average execution time of ESO and IS algorithms reaches about 4240s, while the running time of PSO, GWO, BAS, and AEO are 200s, 500s, 6810s, and 4085s longer than that, respectively. This indicates that ESO can effectively save computation resources compared with other algorithms.

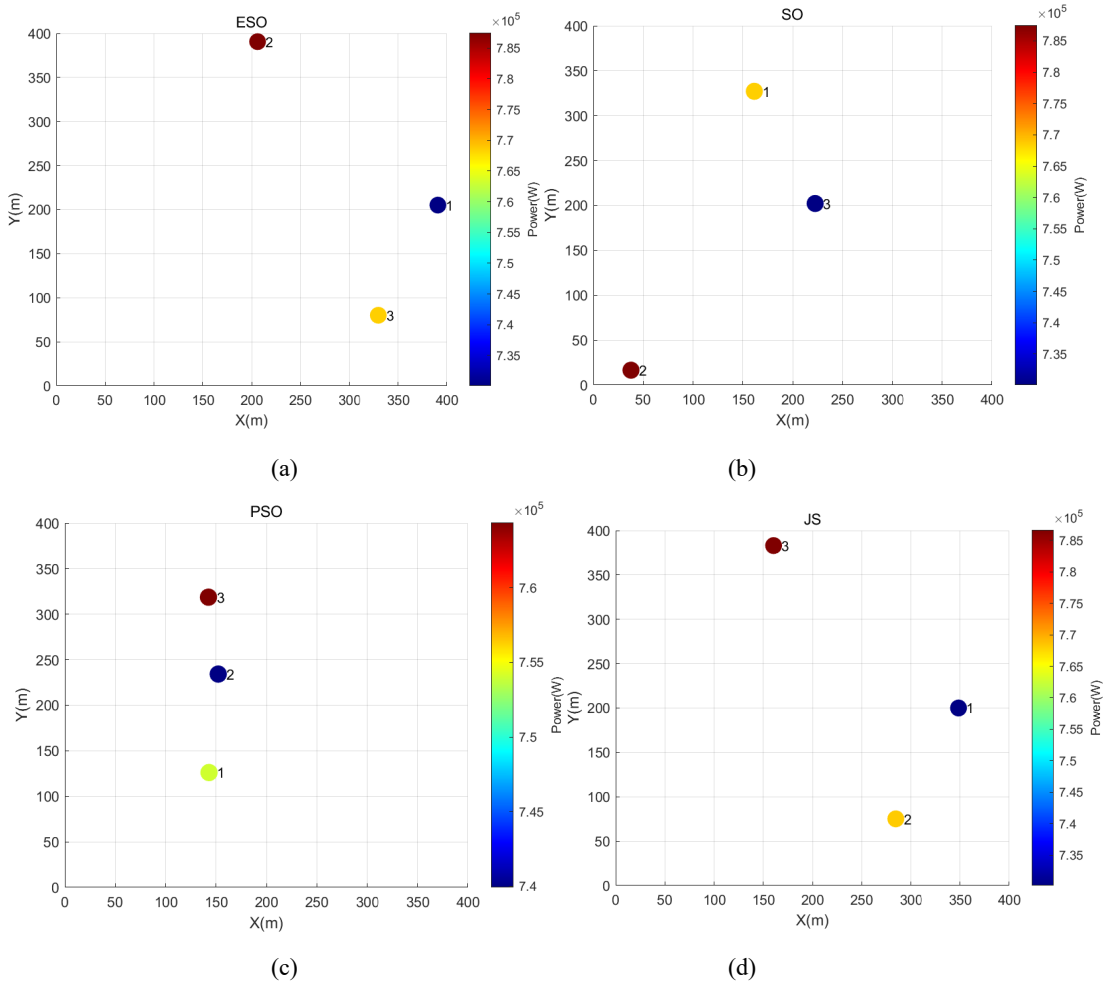

(a) (b)

(c) (d)

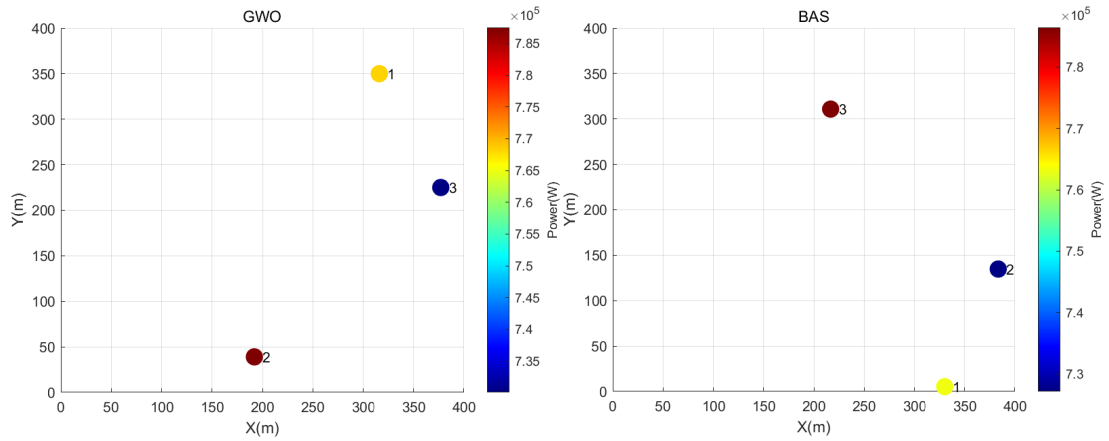

(e) (f)

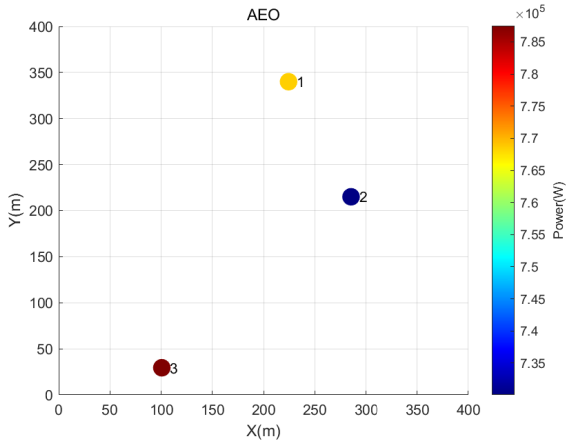

(g)

Fig.4. Optimal layouts acquired by seven algorithms under three buoys array. (a) ESO, (b) SO, (c) PSO, (d) JS, (e) GWO, (f) BAS, and (g) AEO.

5.2 Scenario 2： six buoys array

Scenario 2 studies the array arrangement and optimization of six buoys by seven different algorithms when the sea area is 800*800 m^2.

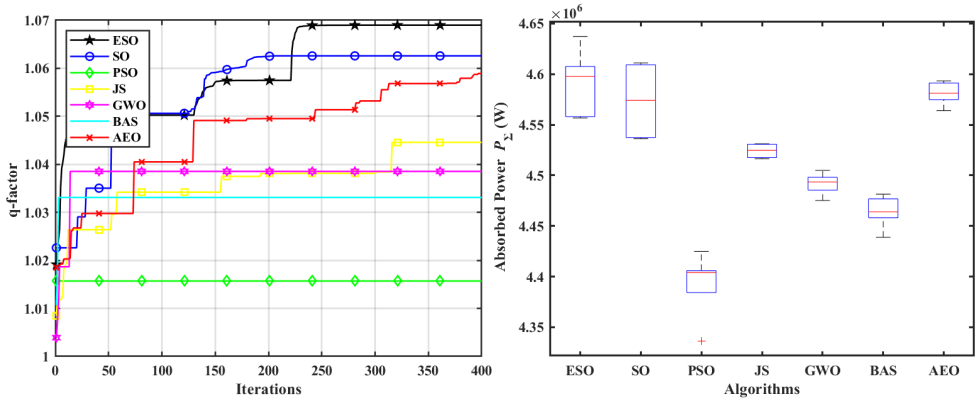

(a) (b)

Fig. 5. Simulation results of seven algorithms under six buoys array. (a) *q* factor and (b) box plot.

Table 6. Simulation results of seven algorithms under six buoys array

Algorithms	Buoy number *i*	*X*/m	*Y*/m	P_i/kW	P_Σ/MW	*q* factor	T_{avg}/s

ESO	1	483.69	51.56	756.813	4.6371	1.069	11400
	2	523.61	290.44	726.166			
	3	680.79	799.26	768.920			
	4	475.87	154.92	811.133			
	5	740.36	675.33	729.592			
	6	423.63	429.23	844.465			
SO	1	230.86	22.88	797.316	4.6093	1.0625	11400
	2	253.27	499.70	763.830			
	3	384.90	188.51	728.760			
	4	150.95	664.84	823.127			
	5	341.14	328.03	740.747			
	6	197.42	781.29	755.506			
PSO	1	64.35	122.59	746.828	4.4059	1.0157	27600
	2	663.29	156.31	744.731			
	3	772.29	718.20	723.792			
	4	381.36	388.98	789.578			
	5	132.45	24.31	691.351			
	6	646.83	607.25	706.960			
JS	1	520.72	498.96	732.249	4.5312	1.0445	32000
	2	475.09	633.83	758.092			
	3	352.46	311.42	741.991			
	4	356.33	791.79	778.333			
	5	289.40	151.64	808.341			
	6	478.27	332.12	712.171			
GWO	1	311.21	684.90	744.647	4.5049	1.0385	16400
	2	68.22	151.13	805.555			
	3	493.46	335.01	739.333			
	4	352.23	552.26	746.573			
	5	477.98	408.34	736.851			
	6	99.29	33.32	731.315			
BAS	1	602.10	240.21	733.738	4.4814	1.0331	71600
	2	76.44	570.89	731.937			
	3	85.96	289.20	754.444			
	4	587.79	575.15	729.003			
	5	284.13	796.88	783.037			
	6	465.08	66.92	748.493			
AEO	1	483.80	760.44	765.989	4.5933	1.0589	55200
	2	631.64	81.925	723.450			
	3	364.10	450.88	833.362			
	4	474.57	280.56	768.362			
	5	93.00	32.178	763.591			
	6	537.89	645.17	738.593			

According to Fig.5 (a), it can be seen that the q factor of the seven algorithms is all larger than

one. In the first 50 iterations, the initial fitness value of the other six algorithms changes dramatically. Among them, the changing speed of ESO is more prominent, and GWO, BAS, and PSO all fall into the local optimal solutions within 50 iterations. Throughout the iteration process, ESO, SO, AEO show relatively strong optimization ability, whereas SO for the intermediate iterations shows a steeper slope of change than that of ESO. Although the convergence speed of ESO is not the fastest among all methods, the comprehensive performance is the best compared to the other six algorithms in terms of overall convergence stability and accuracy.

Figure 5(b) shows the boxplot graph of the absorbed power under the 6-buoy array optimized by various algorithms. Compared with other algorithms, although the upper limit of ESO algorithm is lower than that of SO, the value of the median and the maximum value of the total absorbed power is larger than that of the other five algorithms.

Table 6 tabulates the best positions of WECs under the six buoys scale, the best absorption power, the absorption power of each buoy, and the q factor. It is readily to read that the best absorption power of ESO is the highest, with 4.6371MW, which is 27.8kW, 231.2 kW, 105.9kW, 132.2kW, 155.7kW and 43.8kW higher than SO, PSO, GWO, BAS and AEO, respectively. Meanwhile, regarding the time cost, the average running time cost by SO and ESO can reach 11400s, while PSO, JS, GWO, BAS, and AEO need to execute 16200s, 20600s, 5000s, 60200s, and 43800s longer than that, respectively. Figure 5 shows the optimal layout of the seven algorithms under the optimal absorbed power.

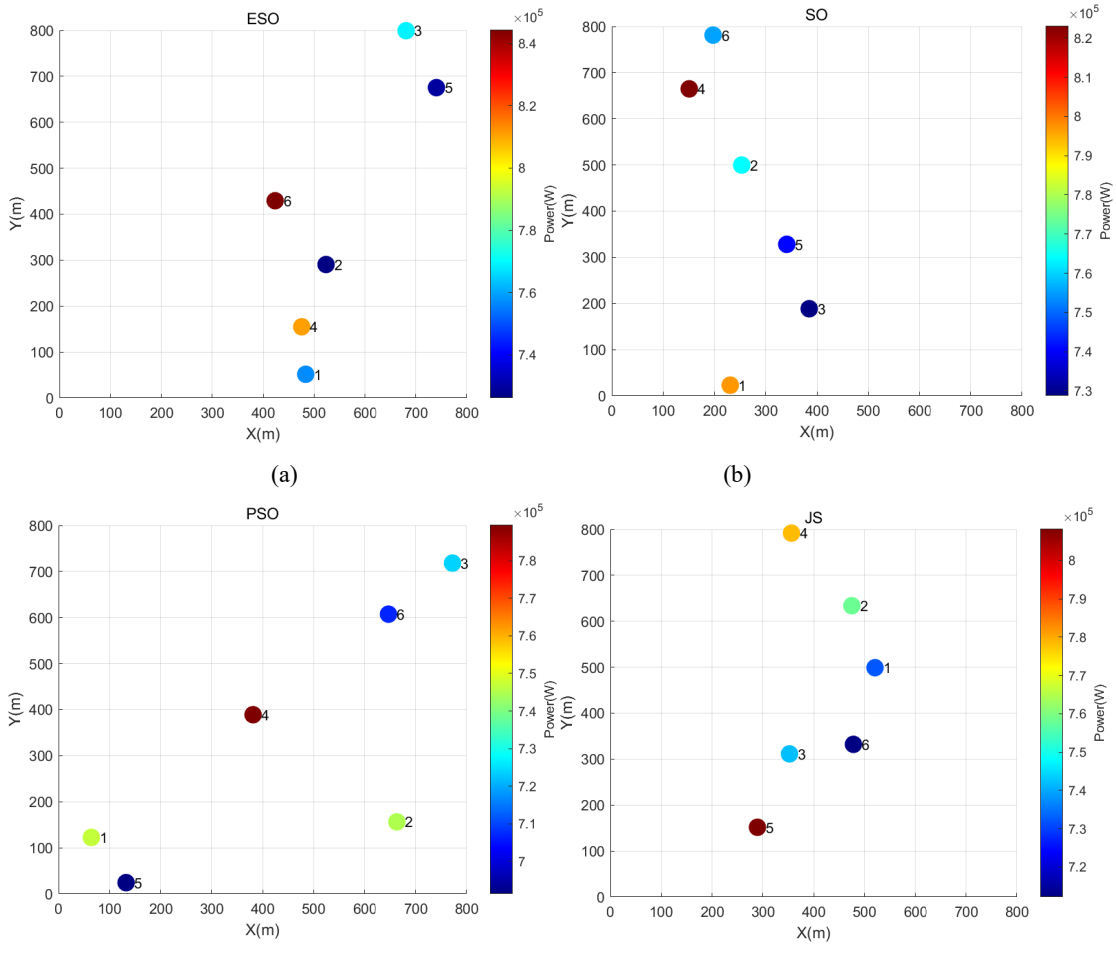

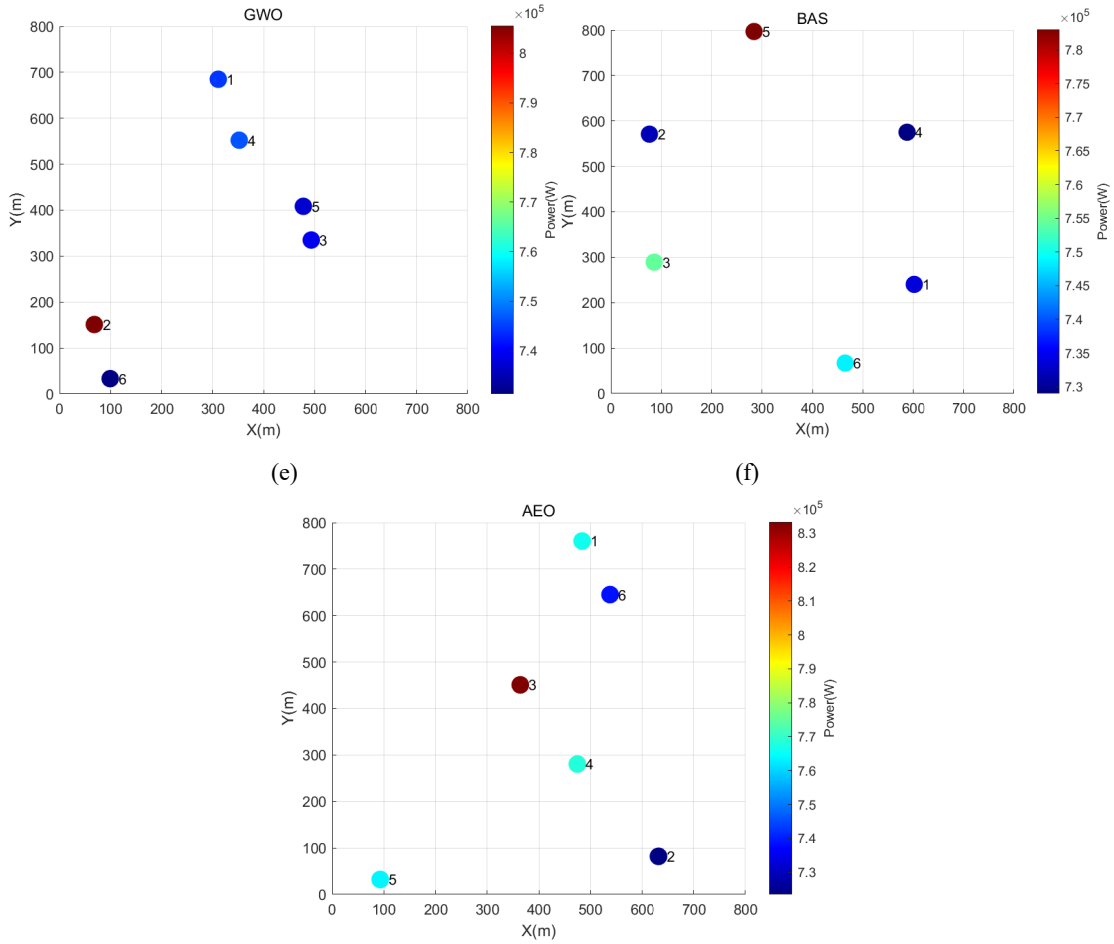

Fig.6. Optimal layouts acquired by seven algorithms under six buoys array. (a) ESO, (b) SO, (c) PSO, (d) JS, (e) GWO, (f) BAS, and (g) AEO.

5.3 Scenario 3： twelve buoys array

Scenario 3 investigates the case of array arrangement and optimization of twelve buoys by seven different algorithms under the sea area is 1600*1600 m^2.

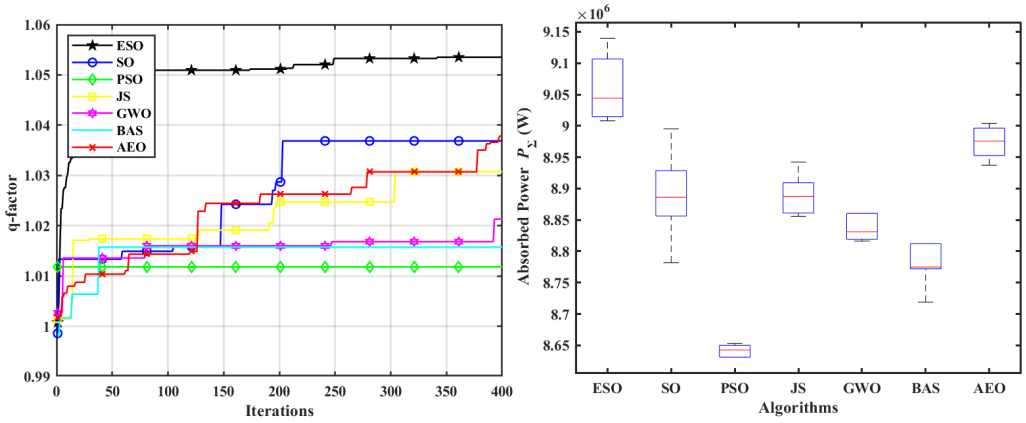

Fig.7. Simulation results of seven algorithms under twelve buoys array. (a) q factor and (b) box plot.

Table 7. Simulation results of seven algorithms under twelve buoys array

Algorithms	Buoy number *i*	*X*/m	*Y*/m	P_i/kW	P_Σ/MW	*q* factor	T_{avg}/s
ESO	1	1521.01	481.53	742.115	9.1397	1.0535	74400
	2	529.47	29.127	771.926			
	3	1401.39	41.40	731.854			
	4	98.85	495.67	767.059			
	5	589.92	1177.30	814.841			
	6	1349.12	842.96	778.174			
	7	968.27	1481.91	740.970			
	8	1330.49	665.53	767.011			
	9	923.34	1596.24	749.471			
	10	1427.06	348.23	782.496			
	11	759.91	1382.11	760.646			
	12	1465.78	995.80	733.160			
SO	1	924.46	1170.33	733.678	8.9954	1.0369	74400
	2	330.63	547.67	761.678			
	3	729.05	390.98	762.498			
	4	536.24	39.608	704.947			
	5	730.76	955.07	766.494			
	6	373.84	1198.47	794.505			
	7	704.95	313.00	714.132			
	8	434.447	692.68	767.877			
	9	625.37	820.85	743.145			
	10	1006.55	9.4219	719.730			
	11	612.80	1542.74	733.096			
	12	562.14	1422.37	793.607			
PSO	1	1224.01	1545.13	722.863	8.6531	0.9974	155000
	2	944.98	131.21	682.280			
	3	288.32	447.89	796.651			
	4	766.21	923	692.330			
	5	636.45	731.68	652.098			
	7	815.03	663.29	781.096			
	6	1256.37	437.48	718.424			
	8	1122.35	865.36	741.775			
	9	142.83	1405.31	654.311			
	10	556.20	1541.96	736.726			
	11	1187.29	1289.36	728.940			
	12	1097.13	133.25	743.159			
JS	1	1481.65	1047.88	721.762	8.9423	1.0307	156000
	2	764.75	1039.80	824.444			
	3	1067.86	1602.75	679.738			
	4	1329.50	461.84	735.702			
	5	1297.40	562.96	787.084			
	7	931.78	276.47	760.863			

	6	950.81	839.19	726.269			
	8	1282.14	1527.80	785.487			
	9	535.34	539.56	743.758			
	10	1401.46	1371.98	713.134			
	11	1123.63	626.90	674.795			
	12	818.07	114.89	766.391			
GWO	1	1562.17	242.24	738.994	8.8605	1.0213	85600
	2	208.63	1214.64	743.075			
	3	862.16	1542.96	708.870			
	4	841.98	381.89	684.732			
	5	705.40	1346.34	785.563			
	7	182.89	9.87	731.994			
	6	248.25	794.72	772.863			
	8	415.92	1563.96	750.231			
	9	220.28	1091.86	743.654			
	10	1435.03	747.81	724.218			
	11	376.79	626.84	720.385			
	12	1559.46	319.33	755.377			
BAS	1	361.29	1263.43	669.680	8.8121	1.0157	324800
	2	1180.62	51.21	714.413			
	3	1552.45	555.43	723.877			
	4	324.13	1009.37	766.961			
	5	878.865	1279.26	746.989			
	7	345.25	705.26	748.412			
	6	606.68	1076.28	804.118			
	8	766.84	1415.95	689.864			
	9	132.58	555.58	739.888			
	10	750.81	246.00	715.521			
	11	553.68	1210.93	775.613			
	12	968.50	1534.19	716.813			
AEO	1	504.43	941.57	713.425	9.0038	1.0378	245200
	2	690.58	1001.39	813.721			
	3	621.51	630.52	759.236			
	4	512.42	753.08	724.384			
	5	1142.71	966.97	745.992			
	7	816.96	416.92	781.699			
	6	951.04	108.28	778.160			
	8	1379.94	116.86	734.106			
	9	1005.41	1387.70	741.223			
	10	829.29	1174.18	752.649			
	11	1253.74	680.42	731.325			
	12	1219.95	340.71	727.889			

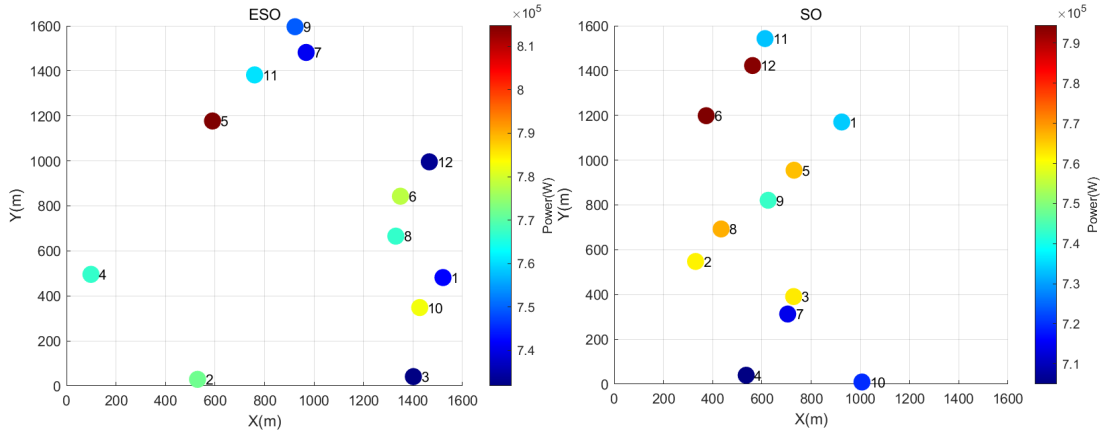

(a) (b)

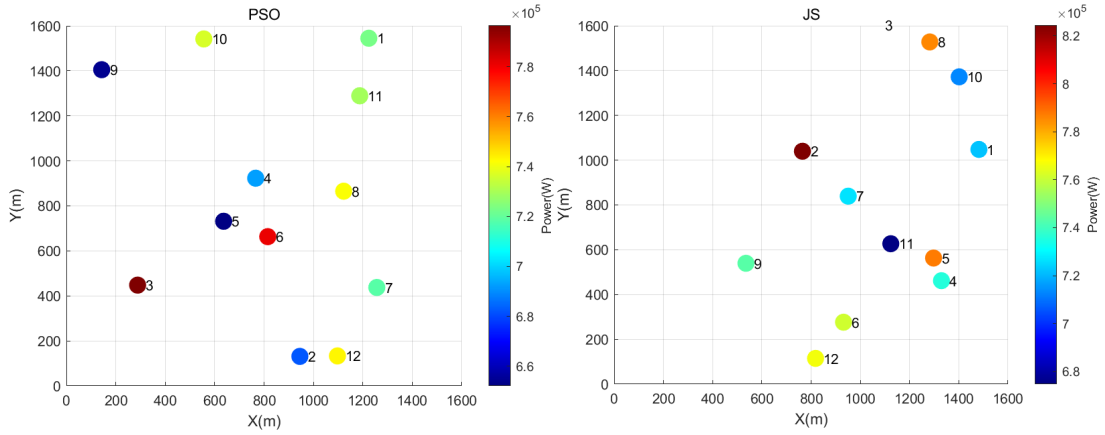

(c) (d)

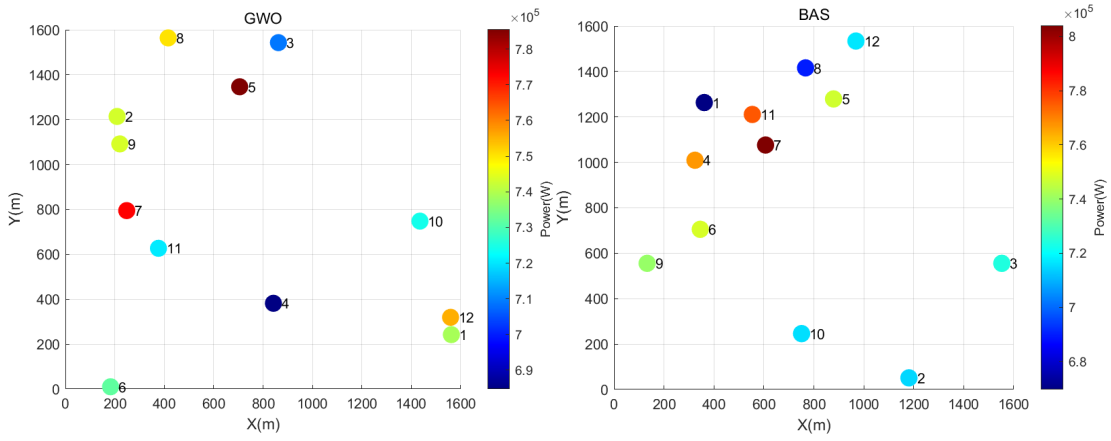

(e) (f)

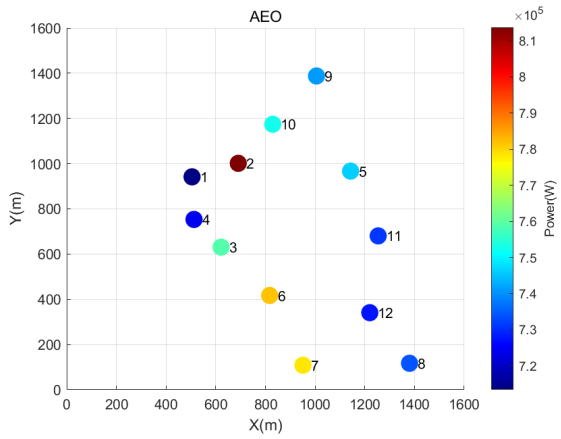

(g)

Fig. 8. Optimal layouts acquired by seven algorithms under six buoys array. (a) ESO, (b) SO, (c) PSO, (d) JS, (e) GWO, (f) BAS, and (g) AEO.

Apparently, the simulation results of seven algorithms under twelve buoys scale are more outstanding than those under three and six scales. According to the q factor changing trajectory under twelve buoy scale in Fig.7 (a), the q factor exceeds 1.04 when ESO executes less than 50 iterations and exceeds 1.05 at the 59th iteration. Meanwhile, the q factor of the other six algorithms never exceeds 1.04, for instance, AEO and GWO both do not converge until 400 iterations, indicating that the ability of both two algorithms to find the global optimum is not strong enough. At the same time, as can be seen from Fig.8 (b), the median, crowd number, and maximum absorption power of ESO are all much higher than those of the other six algorithms.

From the simulation results illustrated in Table 6 and Table 7 under six buoys scale and twelve buoys scale, it is not difficult to see that the larger the scale, the stronger the ESO optimization ability, compared with SO, PSO, JS, GWO, BAS, AEO, the q factor of ESO increases by 1.6%, 5.6%, 2.2%, 3.15%, 3.7% and 1.51%, the maximum absorbed power of ESO increases by 144.337 kW, 486.613 kW, 197.405 kW, 279.248 kW, 327.574 kW and 135.914 kW over SO, PSO, JS, GWO, BAS, and AEO, respectively. Moreover, it can be observed that the average running time of ESO under twelve buoys array is about 74400s, while PSO, JS, GWO, BAS, and AEO cost 80600s, 81600s, 11200s, 250400s, and 170800s longer than that, respectively. The improvement of ESO can considerably improve the efficiency of layout optimization.

6. Conclusions

For the first time, a hybrid wind-wave system is established in this study simultaneously considering the wind turbine proposed in reference [36] and incorporating a three-system WEC system. Then, an ESO is applied to optimize the HWWEC array layout under different sizes. The main conclusions of this work are outlined as follows:

(1) A Vestas V27-225 kW wind turbine model is combined with a three-tether WEC system to build up an HWWEC model. Through the combination of these two models, the utilization rate of the model and environmental resources is able to be greatly improved on the basis of reducing the construction cost;

(2) The original SO is improved to enhance the initial population diversity by introducing the chaotic initialization, meanwhile, asynchronous learning factors and Levy flight are used to

expand the searching range and avoid falling into the local optimal solution, thus the optimization ability is all-round enhanced by ESO. Besides, the introduced mechanism in ESO tends to be more universal and simpler than the original SO, which greatly saves computation resources and improve convergence rate;

(3) Case studies results indicate that for small-scale array arrangement, ESO has the fastest convergence speed and largest power output against its competitors. At the same time, the larger the scale of the system, the ESO optimization performance increases accordingly.

Future studies tend to focus on the following four aspects:

(1) Theoretically, this study verifies that the larger the system's scale, the better the optimization results of ESO. However, for actual operation, the industrial scale could be extremely huge, so future studies will consider and employ scales based on realistic engineering demand to further evaluate the implementation feasibility of ESO in larger HWWEC systems;

(2) Regarding the performance evaluation, this work mainly focuses on maximizing WEC power output and the q factor. In future studies, the evaluation objective function should not be limited only to power output but should also include design objectives, annual energy production, capital, operation, maintenance costs, and environmental impacts to achieve multi-objective optimization;

(3) For a more accurate and comprehensive model analysis, a wider range of oceanic and meteorological conditions tends to be considered during HWWECs array layout optimization. Since waves are random, these uncertainties can have a substantial degrading effect on the power of the WEC, so future work should be extended to adapt to more realistic wave and wind environment;

(4) From a cost-saving perspective, future studies will integrate wind, solar, and gas in the model to optimize power extraction performance under more complex operating conditions.

Acknowledgments

This work was supported by the National Natural Science Foundation of China (62263014) and the Yunnan Provincial Basic Research Project (202201AT070857).

References

[1] Hu, X.Y.; Fang, Y.Z.; Wu, Y.N.; et al. An approach to assess the potential of wave energy resources based on directional energy flux. *Ocean Engineering*, **2023**, 287(1): 115732.

[2] Yang, B.; Li, Y.L.; Li, J.L.; et al. Comprehensive summary of solid oxide fuel cell control: a state-of-the-art review. *Protection and Control of Modern Power Systems*, **2022**, 7(3): 523-553.

[3] Gao, Q.; Bechlenberg, A.; et al. Techno-economic assessment of offshore wind and hybrid wind-wave farms with energy storage systems, *Renewable and Sustainable Energy Reviews*, **2024**, 192: 114263.

[4] Li, X.M.; Zhou, S.W.; Zhao, Y.F. Onshore and offshore wind power generation forecasting using a novel flexible time-varying fractional nonlinear grey model. *Energy Conversion and Management*, **2023**, 297: 117695.

[5] Yang, B.; Liu, B.Q.; Zhou, H.Y.; et al. A critical survey of technologies of large offshore wind farm integration: summary, advances, and perspectives. *Protection and Control of Modern Power Systems*, **2022**, 7(1): 233-264.

[6] Li, C.H.; Han, D.; Chen,Y.J.; et al. Simulation and calculation of maximum transmission power for offshore wind plants accounting for the Electro-Magnetic transient process. *Energy Reports*, **2023**, 9(12): 32-37.
[7] Christopher, J.; Dirk, S. The properties of the global offshore wind turbine fleet. *Renewable and Sustainable Energy Reviews*, **2023**, 186: 113667.
[8] Montaser, M.; Mohammad, A.; et al. Wave energy extraction technologies. *Renewable Energy*, **2024**, 2: 37-51.
[9] Zhou, B.Z.; Wang, Y.; Zheng, Z.; et al. Power generation and wave attenuation of a hybrid system involving a heaving cylindrical wave energy converter in front of a parabolic breakwater. *Energy*, **2023**, 282: 128364.
[10] Chen, Y.J.; Yang, B.; Guo, Z.X.; et al. Dynamic reconfiguration for TEG systems under heterogeneous temperature distribution via adaptive coordinated seeker. *Protection and Control of Modern Power Systems*. **2022**, 7(3): 567-585.
[11] Chandrasekaran, S.; Sricharan, V.V.S. Numerical study of bean-float wave energy converter with float number parametrization using WEC-Sim in regular waves with the Levelized Cost of Electricity assessment for Indian sea states. *Ocean Engineering*, **2021**, 237: 109591.
[12] Zhou, B.Z.; Hu, J.J.; Wang, Y.; et al. Coupled dynamic and power generation characteristics of a hybrid system consisting of a semi-submersible wind turbine and an array of heaving wave energy converters. *Renewable Energy*, **2023**, 214: 23-38.
[13] Ren, N.X.; Ma, Z.; Fan, T.H.; et al. Experimental and numerical study of hydrodynamic responses of a new combined monopile wind turbine and a heave-type wave energy converter under typical operational conditions. *Ocean Engineering*, **2018**, 159: 1-8.
[14] Michele, S.; Renzi, E.; Perez-Collazo, C.; et al. Power extraction in regular and random waves from an OWC in hybrid wind-wave energy systems. *Ocean Engineering*, **2019**, 191: 106519.
[15] Zhao, Z.N.; Zhang, Z.; Xu, L.X.; et al. Tumbler-shaped hybrid triboelectric nanogenerators for amphibious self-powered environmental monitoring. *Nano Energy*, **2020**, 76: 104960.
[16] Wang, B.H.; Deng, Z.W.; Zhang, B.C. Simulation of a novel wind-wave hybrid power generation system with hydraulic transmission. *Energy*, **2022**, 238: 121833.
[17] Ti, Z.L.; Deng, X.W. Layout optimization of offshore wind farm considering spatially inhomogeneous wave loads. *Applied Energy*, **2022**, 306: 117947.
[18] Alireza, S.; Mohammad, R.N.; Talal, E.; et al. A multi-objective approach for location and layout optimization of wave energy converters. *Applied Energy*, **2023**, 347: 121397.
[19] Golbaz, D.; Asadi, R.; Amini, E.; et al. Layout and design optimization of ocean wave energy converters: A scoping review of state-of-the-art canonical, hybrid, cooperative, and combinatorial optimization methods. *Energy Reports*, **2022**, 8: 15446-15479.
[20] Lyu, J.Y.; Abdelkhalik, O.; Lucia Gauchia, L. Optimization of dimensions and layout of an array of wave energy converters. *Ocean Engineering*, **2019**, 192: 106543.
[21] Neshat, M.; Mirjalili, S.; Sergiienko, N.Y.; et al. Layout optimisation of offshore wave energy converters using a novel multi-swarm cooperative algorithm with backtracking strategy: A case study from coasts of Australia. *Energy*, **2022**, 239: 122463.
[22] Zhang, B.S.; Song, B.W.; Mao, Z.Y.; et al. A novel wake energy reuse method to optimize the layout for Savonius-type vertical axis wind turbines. *Energy*, **2017**, 121: 341-355.
[23] Kaya, B.; Oğuz, E. Investigation of layout optimization for offshore wind farms and a case study for a region in Turkey. *Ocean Engineering*, **2022**, 266: 112807.
[24] Falnes, J. Radiation impedance matrix and optimum power absorption for interacting oscillators in surface waves. *Applied Ocean Research*, **1980**, 2(2): 75-80.

[25] Falnes, J.; Budal, K. Wave-power absorption by parallel rows of interacting oscillating bodies. *Applied Ocean Research*, **1982**, 4(4): 194-207.

[26] Silvia, B.; Marianna, G.; Adri à , M.M.; et al. Wave energy farm design in real wave climates: the Italian offshore. *Energy*, **2017**, 122: 378-389.

[27] Jin, P.; Zheng, Z.; et al. Optimization and evaluation of a semi-submersible wind turbine and oscillating body wave energy converters hybrid system, *Energy*, **2023**, 282: 128889.

[28] Ghafar, H.R.; Ghassemi, H.; et al. Power matrix and dynamic response of the hybrid Wavestar-DeepCwind platform under different diameters and regular wave conditions, *Ocean Engineering*, **2022**, 247: 110734.

[29] Astariz, S.; Perez-Collazo, C.; Abanades, J.; et al. Towards the optimal design of a co-located wind-wave farm. *Energy*, **2015**, 84: 15-24.

[30] Yang, B.; Wu, S.C.; Zhang, H.; et al. Wave energy converter array layout optimization: A critical and comprehensive overview. *Renewable and Sustainable Energy Reviews*, **2022**, 167: 112668.

[31] Wang, Y.T.; Yang, B. Optimal PV array reconfiguration under partial shading condition through dynamic leader based collective intelligence. *Protection and Control of Modern Power Systems*, **2023**, 8(3): 646-661.

[32] Eikrem, K.S.; Lorentzen, R.J.; Faria, R.; et al. Offshore wind farm layout optimization using ensemble methods. *Renewable Energy*, **2023**, 216: 119061.

[33] Sharp, C.; DuPont, B. Wave energy converter array optimization: A genetic algorithm approach and minimum separation distance study. *Ocean Engineering*, **2018**, 163: 148-156.

[34] He, Z.C.; Ning, D.Z.; Gou,Y; et al. Optimization of a wave energy converter square array based on the differential evolution algorithm. *Ocean Engineering*, **2022**, 262: 112189.

[35] Simley, E.; Angelou, N.; Mikkelsen, T.; et al. Characterization of wind velocities in the upstream induction zone of a wind turbine using scanning continuous-wave lidars. *Journal of Renewable & Sustainable Energy*, **2016**, 8(1): 013301.

[36] Wu, J.; Shekh, S.; Sergiienko, N.Y.; et al. Fast and effective optimization of arrays of submerged wave energy converters. In: 2016 Proceedings of the Genetic and Evolutionary Computation Conference (GECCO). 20 July **2016**, Denver, USA, pp: 1045-1052.

[37] Hashim, F.A.; Hussien, A.G. Snake Optimizer: A novel meta-heuristic optimization algorithm. *Knowledge-Based Systems*, **2022**, 242: 108320.

[38] Syama, S.; Ramprabhakar, J.; Anand, R.; et al. A hybrid extreme learning machine model with levy flight chaotic whale optimization algorithm for wind speed forecasting. *Results in Engineering*, **2023**, 19: 101274.

[39] Jaramillo, O.; Borja, M.A. Bimodal versus Weibull wind speed distributions: An analysis of wind energy potential in La Venta Mexico. *Wind Engineering*, **2004**, 28: 225-234.

[40] Kale, B.; Buckingham, S.; et al. Comparison of the wake characteristics and aerodynamic response of a wind turbine under varying atmospheric conditions using WRF-LES-GAD and WRF-LES-GAL wind turbine models, *Renewable Energy*, **2023**, 216: 119051.

[41] Rony, J.S.; Karmakar, D. Coupled dynamic analysis of hybrid offshore wind turbine and wave energy converter. *Journal of Offshore Mechanics and Arctic Engineering*, **2022**, 144(3): 1-13.

[42] Hamid, R.G.; Hassan, G.; Alireza, A.; et al. Novel concept of hybrid wavestar-ffoating offshore wind turbine system with rectilinear arrays of WECs. *Ocean Engineering*, **2022**, 266: 112253.

[43] Homayoun, E.; Panahi, S.; Ghassemi, H.; et al. Power absorption of combined wind turbine and wave energy converter mounted on braceless floating platform. *Ocean Engineering*, **2022**, 266: 113027.